New Scaling Law for Turbulent Boundary Layers with High Surface Mass Transfer

Rozie Zangeneh[1], Paul E. DesJardin[1], and James Chen [1,*]
[1]*Department of Mechanical and Aerospace Engineering, The State University of New York, Buffalo, NY, USA*
[*]*Corresponding author: chenjm@buffalo.edu*

A fundamental understanding of the phenomena occurring in the turbulent boundary layer in the presence of surface blowing is limited, and considerable disagreements persist even in describing primary quantities, such as the boundary layer profile. The theories based on the linear boundary layer equations show that the thickness of the sublayer increases in the presence of surface blowing; therefore, the viscous sublayer and law of the wall modify. In this study, direct numerical simulations (DNS) of turbulent boundary layers with uniform surface mass transfers are carried out in order to scale the velocity profile. Emphasis is placed on moderate to high mass transfer rates, which are relevant to the most common hybrid rocket configuration. DNS data is used to establish a functional law of the wall and a law of wake by means of the relation between the wall shear stress and surface mass transfer. Analysis of the mean kinetic energy budget shows that the magnitude of turbulent kinetic energy increases by surface mass transfer, and the production rate extends significantly in the inner layer as the injection rate increases. DNS data of various surface blowing is used to complete the closure of turbulence kinetic energy equation and develop an eddy viscosity model. The predicted turbulent kinetic energy and eddy viscosity agree with DNS data for moderate to high blowing rates.

I. Introduction

Wall-bounded turbulent boundary layers with mass transfer have been the subject of theoretical and technological studies. Some of the applications include turbulent drag reduction, thermal protection, and flow induction by gas injection in reacting boundary layers of combustion processes. In particular, in many combustion applications, burning becomes tightly completed with conjugate heat and mass transfer processes from the surface of the fuel; hence, the effect of surface blowing should be considered in modeling such combustion systems. One of the notable combustion systems involving surface blowing is hybrid rockets. Such rockets are promising alternatives to liquid or solid propellant rockets, owning to combining the benefits of solid and liquid rockets in one stand. The propellants are stored in two different states of matter in a hybrid rocket. Accordingly, the fuel is solid and the oxidizer is a gas/liquid, providing a highly dense fuel source similar to a propellant solid motor, yet with the throttle control of a liquid motor [1, 2]. In

hybrid rocket motors, the effect of surface blowing from the liquefying fuel could become significant, coupled with chemical reactions, making the model highly non-linear [3]. Therefore, in order to develop effective prediction tools for hybrid rockets and similar configurations, turbulent boundary layers with mass transfer needs to be well understood.

In classical non-transpirational turbulent boundary layers, there is a well-established Van Driest law of the wall. It can be derived from inner layer similarity arguments leading to a "mixing-length" formula for the mean velocity, $l = \kappa y[1 - exp(-y/A)]$ [4]. There have been many attempts to adjust or modify the length scale; in particular, some modified it to calculate flows with mass transfer and pressure gradient. Kays et al. [5] modified the wall damping, A, as a function of transverse velocity and pressure gradient. Nicoll et al. [6] extended the Van Driest model to include the effect of mass transfer. Their approach was based on the solution of Stokes flow with mass transfer term. Tennekers [7] obtained a new semi-logarithmic law of wall for a velocity defect law, assuming the inner and outer regions have a joint velocity scale. Cebeci et al. [8] extended the Van Driest modeling of sublayer to flows with mass transfer and heat transfer by modifying the eddy viscosity in the inner region. A new bi-logarithmic law of the wall for blowing surfaces was obtained in the 1950s (Mickley et al. [9]; Black et al. [10]) using mixing-length theory. Stevenson [11] proposed generalized forms of the law of the wall and, shortly afterward, a velocity defect law for the turbulent boundary layer with suction and blowing at zero pressure gradient for small transpiration velocities. Marxman et al. [12, 13] investigated the turbulent boundary layer with heat transfer, mass transfer, and chemical reactions theoretically, which is relevant to the boundary layer of the combustion process in hybrid engines. They formulated the reduction in skin friction caused by the surface mass addition.

Blowing walls are also investigated through measurements. Anderson [14] conducted an experimental investigation of transpired turbulent boundary layers for adverse pressure gradients. A new wall law was introduced by obtaining the best fit to the logarithmic region of experimental velocity profiles. Squire [15] measured turbulent boundary layers with air injection and found that a clearly defined law of the wall exists. He calculated the mixing-length constant from measured data. More recently, Ferro [16] provided new experimental data on suction and blowing boundary layers. It was reported that the suction wall modifies the mean velocity profile with an extended logarithmic layer and without a distinctive wake region, and wall-blowing enhances the intensity of the velocity fluctuations, especially in the outer region. Despite substantial theoretical and experimental work, Direct Numerical Simulations of wall-bounded flows with mass injections are limited. One of the earliest DNS works was the fully developed turbulent channel flow with surface injection and suction by Sumitani et al. [17]. They found that the wall-blowing decreases the friction coefficient; however, tends to enhance the near-wall turbulence intensity such that the Reynolds stresses and turbulent heat fluxes are increased, whereas the suction has an inverse impact. Pure analytical work was conducted by Vigdorovich et al. [18] using the method of matched asymptotic expansion to construct a solution for the near-wall and core region of Poiseuille flow; however, no DNS was conducted to scale the velocity. Avsarkisov et al. [19, 20] investigated the mean velocity

law of the Poiseuille flow with wall transpiration using the two-point correlation (TPC) method to find mean velocity scaling laws and used DNS to establish a relation between profiles.

With the renewed interest in hybrid rockets, an appropriate wall model is required to account for the surface blowing from the fuel for high-fidelity computational fluid dynamics (CFD) simulations. Large-eddy simulation (LES) of turbulent flows attempts to reduce the grid points necessary to compute a turbulent flow by modeling the small scales and resolving only the large, energy-carrying structures. It has been argued that extending LES to practical applications is not feasible if the wall layer is fully resolved since it prohibitively increases the required computational effort [21, 22]. For flows of engineering interest, it is desirable to utilize approximate boundary conditions such that the wall stress is not computed directly but is defined in terms of the velocity in the core of the flow. This approach allows one to place the first grid point in the logarithmic region, thus avoiding simulating the wall layer [23, 24]. The subgrid-scale structures in the outer region of the boundary layer, which are known to be nearly isotropic compared to those near the wall, are less computationally intense to model. Note that to represent the effect of the wall layer on the turbulent core of the flow, the approximate boundary condition must model the interaction between the inner and outer layers. Therefore it is necessary to scale the full profile of the boundary layer. To date, no DNS has been conducted to scale the full profile of turbulent boundary layers with high transpiration rates; $V_w^+ \gtrsim 0.2$. Therefore, this study conducts DNS of a zero-pressure gradient (ZPG) turbulent boundary layer to establish a functional boundary layer scaling for moderate to high-blowing surfaces in order to model the wall stress. Another approach would be the class of wall models that switch to a Reynolds-averaged Navier-Stokes (RANS) model in the inner layer [25, 26]. In this approach, the wall is resolved in the RANS context to model the eddy viscosity in the inner layer. Developing eddy viscosity models require insights into the turbulence structures near the surface. However, a fundamental understanding of the turbulence phenomena occurring in the boundary layer in the presence of wall-blowing is limited [27]. To the authors' best knowledge, no turbulence closure model was developed for a wall model that takes into account the effect of surface mass injections. In the second part of this study, efforts are made to formulate and validate a functional eddy viscosity model using DNS data of various surface blowing rates. The model can be used to develop wall-modeled LES of turbulent boundary layers involving surface blowing.

In the section that follows the numerical method and details of DNS for the velocity scaling law are provided to develop a wall stress model. In Section III, The mean turbulent kinetic energy budget is analyzed for various blowing rates to develop an eddy viscosity model for the inner region of the boundary layer. Results are discussed, and comparisons are made to validate the models.

II. Wall Stress Model

A. Velocity Scaling Law

Van Driest [4] approximated the mean momentum equation of compressible flow in a ZPG turbulent boundary layer as:

$$-\frac{\overline{\rho u' v'}}{\partial y} + \mu \frac{\partial^2 U}{\partial y^2} = \rho V \frac{\partial U}{\partial y}. \tag{1}$$

Integrating Eq. (1), one may obtain,

$$-\overline{\rho u' v'} + \mu \frac{\partial U}{\partial y} = \rho V_w U + \tau_w, \tag{2}$$

where μ is the dynamic viscosity, ρ is the flow density, U and V are the streamwise and transverse mean velocity of flow, and τ_w is the wall shear stress. Following Vigdorovich [18] method, which is developed for incompressible Poiseuille flow, we formulated closure conditions for the ZPG compressible turbulent boundary layer, assuming the problem depends on a finite number of governing parameters,

$$\frac{\partial U}{\partial y} = F_1 \left(y, \mu, \delta, V_w, u_\tau \right), \tag{3}$$

$$\overline{\rho u' v'} = F_2 \left(y, \mu, \delta, V_w, u_\tau, \rho \right), \tag{4}$$

where u_τ is the friction velocity and δ is the boundary layer thickness. Solving Eq. (3) for u_τ and substituting in Eq. (4) leads to,

$$\overline{\rho u' v'} = F_3 \left(y, \frac{\partial U}{\partial y}, \mu, \delta, V_w, \rho \right). \tag{5}$$

Differentiating Eq. (3) leads to,

$$\frac{\partial^2 U}{\partial^2 y} = \frac{\partial F_1(y, \mu, \delta, V_w, u_\tau)}{\partial y}. \tag{6}$$

Solving Eqs. (3) and (6) for u_τ and V_w and substituting in Eq. (5) gives,

$$\overline{\rho u' v'} = F_4 \left(y, \mu, \delta, \frac{\partial U}{\partial y}, \frac{\partial^2 U}{\partial^2 y}, \rho \right). \tag{7}$$

Equation (5) can be used for the near-wall region, where the outer scale of the flow, the boundary layer thickness, is less relevant. By applying dimensional consideration:

$$\overline{\rho u' v'}|_{near-wall} = -\left(y\frac{dU}{dy}\right)^2 S_0(Re, \beta), \tag{8}$$

where $Re = \frac{\rho y^2}{\mu}\frac{dU}{dy}$ and $\beta = \frac{V_w \phi(Re)}{y}(\frac{dU}{dy})^{-1}$. Eq. (8) relates the shear stress to the mean velocity gradient. Since the dependence of this relationship on the transverse velocity, V_w, must weaken by moving away from the wall, the parameter β is defined so that the function $\phi(Re)$ has the asymptotic behavior away from the wall, near the edge. On the other hand, near the edge, molecular viscosity exerts no influence on mean fluid motion, Eq. (7) can be used; applying dimensional consideration and assuming F_4 is independent of μ gives,

$$\overline{\rho u' v'}|_{near-edge} = -\frac{y^2(\delta - y)^2}{\delta^2}\left(\frac{dU}{dy}\right)^2 S_1(\eta, \gamma), \tag{9}$$

where $\eta = y/\delta$ and $\gamma = \rho(y - \delta)\frac{d^2U}{dy^2}(\frac{dU}{dy})^{-1}$. Combining Eqs. (8) and (9) gives,

$$\overline{\rho u' v'} = -\frac{y^2(\delta - y)^2}{\delta^2}\left(\frac{dU}{dy}\right)^2 S(Re, \beta, \eta, \gamma), \tag{10}$$

where S combines S_0 and S_1 functions. Substituting in Eq. (2), non-dimensionalizing, and using wall parameters, $U^+ = U/u_\tau$, $V_w^+ = V_w/u_\tau$, and $R_\tau = \rho u_\tau \delta/\mu$ leads to,

$$\eta^2(1-\eta)^2\left(\frac{dU^+}{d\eta}\right)^2 S(Re, \beta, \eta, \gamma) + \frac{1}{Re_\tau}\frac{dU^+}{d\eta} = 1 + V_w^+ U^+ - 2\eta. \tag{11}$$

Introducing the small parameter $\epsilon = (\ln Re_\tau)^{-1}$ and assuming that $V_w^+ = \epsilon m$, $m = O(1)$, an asymptotic solution can be found for $\epsilon \to 0$, i.e., in the limit of high values of the logarithm of the Reynolds number, Re_τ, and at small values of transpiration velocity. Eq. (11) is generic and applied to near-wall and near-edge regions. Near the edge of the boundary layer, we seek the solution to the problem in the following form,

$$U_e^+ = \frac{d_0}{\epsilon} + d_1 + O(\epsilon), \quad U = U_e^+ + \Phi(\eta) + O(\epsilon), \tag{12}$$

where U_e^+ is the dimensionless maximum mean velocity and d_0, d_1 are coefficients. Substituting this in Eq. (11), and taking the limit as $\epsilon \to 0$ we obtain,

$$\eta^2(1-\eta)^2\left(\frac{d\Phi}{d\eta}\right)^2 S(\infty,\beta,\eta,\gamma)+\frac{1}{Re_\tau}\frac{d\Phi}{d\eta}=1+md_0-2\eta. \tag{13}$$

For the second-order differential equation, we set two initial conditions at the point of maximum mean velocity, namely $\Phi(U_e^+)=\Phi'(U_e^+)=0$. Near the core region, $Re_\tau\to\infty$ and the solution to Eq. (13) has the following asymptotic behavior,

$$\Phi=\frac{\sqrt{1+md_0}}{\chi}\left[\ln\eta+A(\sqrt{1+md_0})+O(\eta^\alpha)\right]\quad \eta\to 1, \tag{14}$$

where $\chi=\sqrt{S}$.

1. Wall Region

By introducing the wall variable, $y^+=\rho y u_\tau/\mu=\eta Re_\tau$, Eq. (11) can be rewritten in the limit of $Re\to\infty$ as follows,

$$\left(y^+\frac{dU^+}{dy^+}\right)^2 S(\infty,\beta,\eta,\gamma)+\frac{dU^+}{dy^+}=1+V_w^+U^+. \tag{15}$$

The velocity has a logarithmic asymptotic behavior at the outer boundary of the wall region:

$$U^+=\frac{1}{\chi}\left[lny^+ + C_0\right]+O((y^+)^{-\alpha})\quad y^+\to\infty. \tag{16}$$

Thus, the quantity χ, defined by Eq. (16) is the von Karman constant. In the general case of a non-zero transpiration velocity, by using new variables, $Y=V^+y^+$, $W=\frac{2}{V^+}\sqrt{1+V^+U^+}$ Eq. (15) may be transformed to,

$$\left(Y\frac{dW}{dY}\right)^2 S(Re,\beta,\eta,\gamma)+\frac{2}{W}\frac{dW}{dY}=1. \tag{17}$$

Since in the outer part of the wall region, the Reynolds number is high, we have,

$$W=\frac{1}{\chi}lnY+C_1(V_w^+)+O(Y^{-\alpha}), \tag{18}$$

where C_1 is a function of integration. After casting back to the original variables, Eq. (18) yields an asymptotic representation of the velocity profile:

$$\frac{2}{V_w^+}\left(\sqrt{1+V_w^+U^+}-1\right)=\frac{1}{\chi}\left[lny^+ + c(V_w^+)\right]+O(y^{-\alpha}), \tag{19}$$

Equation (19) extends the logarithmic law, Eq. (16) in the case of surface mass transfer since it must reduce to Eq. (16) when $V_w^+ = 0$.

2. Velocity Defect Law

The function Φ in Eq. (14) describes the mean velocity profile in the core region. The scaling law of Eq. (19) is valid in the wall regions outside the viscous sublayers. In what follows, we will unify both these representations and will derive a composite version that holds true over the entire boundary layer, from the viscous layer to the velocity defect region. Rewriting scaling law, Eq. (19), in outer variables leads to,

$$\frac{2}{V_w^+}\left(\sqrt{1+V_w^+U_e^+ + V_w^+\Phi(\eta)} - 1\right) = \frac{1}{\chi}\left[\ln\eta + lnRe_\tau + c(V_w^+)\right]. \tag{20}$$

The second term under the square root on the left-hand side of Eq. (20) is of the order of unity, while the third is of the order of ϵ. Expanding the left-hand side of Eq. (20) gives,

$$\frac{2}{V_w^+}\left(\sqrt{1+V_w^+U_e^+} + \frac{\Phi(\eta)}{\sqrt{1+V_w^+U_e^+}}\right) = \frac{1}{\chi}\left[ln\eta + lnRe_\tau + c(V_w^+)\right] + O(\epsilon). \tag{21}$$

Substituting the function Φ for its asymptotic expansion from Eq. (14) in this relation and equating similar terms leads to,

$$\frac{2}{V_w^+}\left(\sqrt{1+V_w^+U_e^+} - 1\right) = \frac{1}{\chi}\left[lnRe_\tau - A(\sqrt{1+V_w^+U_e^+}) + c(V_w^+)\right] + O(\epsilon). \tag{22}$$

Then subtracting from Eq. (20) leads to,

$$\frac{2}{V_w^+}\left(\sqrt{1+V_w^+U^+} - \sqrt{1+V_w^+U_e^+}\right) = \frac{\Phi(\eta)}{\sqrt{1+V_w^+U_e^+}} + c(V_w^+). \tag{23}$$

This enables the solution to Eq. (13) to be applicable to a wider region, extending this region to the wall. In Eq. (13), $S = \kappa^2$ and related to the von Karman constant, which is modified to $\kappa[1 - exp(-y^+/A^+)]$in the presence of the wall by Van Driest [4], where $A^+ = 26\,(\tau/\tau_w)^{-1/2}$. Cebeci et al. [8] modified the wall-damping length scale in the presence of pressure gradient and mass transfer to,

$$A^+ = 26\left[-\frac{p^+}{V_w^+}[exp(11.8V_w^+) - 1] + exp(11.8V_w^+)\right]^{-1/2}. \tag{24}$$

3. Wake Law

The Coles law of wake is given by: $\frac{\Pi}{\kappa} W\left(y/\delta\right)$, where the function W provides the self-similar shape of the velocity profile in the outer flow, and the function Π is used to change the amplitude of the outer velocity profile. Coles [28] suggested $W = 2\sin 2\left(\left(\frac{\pi}{2}\right)\left(\frac{y}{\delta}\right)\right)$, as a good choice for the wake-like shape of the outer. In the case of surface mass transfer, we propose a new wake law, which is suitable for the shape of the outer boundary for the proposed velocity scaling law: $\frac{b}{\kappa}(\eta - \sin^{\alpha}\frac{\pi}{2}\eta)$. By adding the wake law to Eq. (23), we can introduce the following velocity scale, U^*,

$$U^* = \frac{2}{V_w^+}\left(\sqrt{1+V_w^+U_e^+} - \sqrt{1+V_w^+U^+}\right) = -\frac{\Phi(\eta)}{\sqrt{1+V_w^+U_e^+}} - c(V_w^+) + \frac{b}{\kappa}\left(\eta - \sin^{\alpha}\frac{\pi}{2}\eta\right). \tag{25}$$

This model contains five free parameters. To adjust the rate of wall damping, we rewrite $\sqrt{S}$ in Eq. (13) as $\kappa[1 - exp(-(y^+/A^+)^m)]$, where Eq. (24) is used for A^+ for a ZPG case. κ is closely related to the von Karman constant and is essentially equivalent to the one in the wake law, Eq. (25). Together (κ, m) define the overall size of the wall layer from the viscous sublayer through the buffer layer to the end of the logarithmic region as suggested by Cantwell [29]. c sets the blowing rate dependent function in Eq. (25). b defines a length scale for the region where wake-like behavior begins, and the exponent α helps shape the outer part of the profile. The model parameters $(m, \kappa, c, b, \alpha)$ for the profile scaling model in Eq. (25) are selected by minimizing the total squared error between a given blowing data profile and the velocity profile,

$$J = \frac{1}{N}\sum_{n=1}^{N}\left(U^*(m,\kappa,c,b,\alpha,y_i^+) - U_i^*(y_i^+)\right)^2, \tag{26}$$

where N is the number of data points in a given profile, optimal parameters are defined as values that produce a minimal squared error for each DNS data. A similar approach has been used to find optimal parameters for a universal velocity profile with no mass transfer [30].

B. DNS of Turbulent Boundary Layer with Surface Mass Transfer

1. Simulation Setup

In order to verify the scaling law to be formulated for the velocity profile of the moderate to high blowing surfaces, the DNS of ZPG turbulent boundary layer was conducted with various blowing rates, where the blowing parameter is defined as,

$$B = \frac{\rho_w V_w U_e}{\tau_w}. \tag{27}$$

Table 1. Flow parameters for DNS of a flat plate.

B	Re_τ	$\frac{V_w}{u_e}$	V_w^+
1	1435	0.0013	0.038
2	1407	0.0024	0.073
3	1325	0.0037	0.112
6	1284	0.0057	0.182
10	1137	0.0092	0.298
14	1105	0.0137	0.443
20	1067	0.0195	0.627

A schematic of the flow over a flat plate is presented in Fig. 1 to show the physical and computational domains. A long computational domain is considered with $L_x = 86\delta$ $L_y = 10\delta$, and $L_z = 6\delta$ in the streamwise x, wall-normal y and spanwise z directions. The grid resolution in the wall-parallel direction is held constant at $x^+ \approx z^+ = 5.6$. In the wall-normal direction, the grid is smoothly stretched, and the first grid size is located off the wall such that $y^+ = 0.7$. To prescribe fully turbulent inflow boundary conditions, synthetic turbulence was generated using the digital filter method [31]. The periodic boundary condition is imposed in the spanwise direction. After sweeping the initial transient flow ($100t_c$), statistics are sampled for a period covering $200t_c$, where $t_c = \delta/U_e$. Each simulation is performed using 4000 processors, for a total of approximately 216K CPU hours. The CFL number is kept below 0.8. Fluid is blown through the wall in the vertical direction.

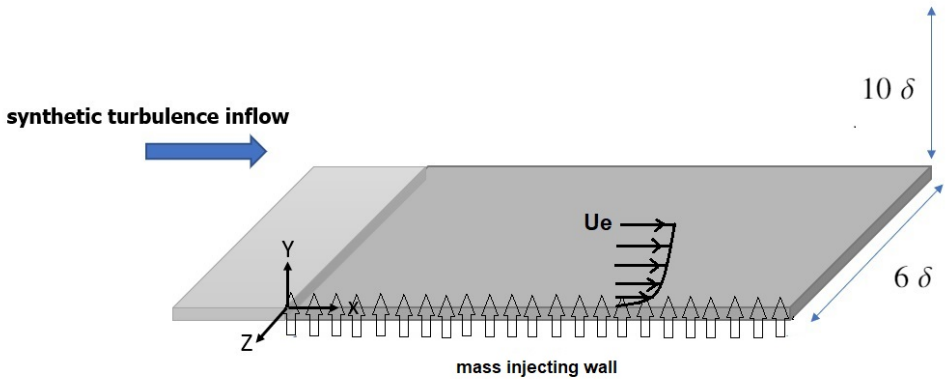

Figure 1. Schematic view of computation domain. Fluid is blown through the lower wall at a constant rate.

Various blowing levels are considered to compare the theory with DNS, up to $B = 20$. The turbulent Reynolds number for no injection case is $Re_\tau \approx 1550$; however, Re_τ decreases with increasing the blowing level. Table 1 shows the complete summary of the flow and simulation parameters for DNS. For the present work, we employ a compressible flow solver, ABLATE, which is an open-source software package being developed by the Center for

Hybrid Rocket Exascale Simulation Technology (CHREST) to simulate hybrid rocket motors at exascale [32]. The code solves compressible Navier-Stokes using a finite volume formulation, where the AUSM+up algorithm is used to calculate the convective fluxes [33]. Runge–Kutta scheme is used for temporal discretization. The code is validated in previous works of the center [34, 35].

Primary, DNS of a turbulent boundary layer is conducted for a zero blowing surface as a base case in order to validate the simulation setup and computational domain. Fig. 2 illustrates the iso-surface of swirling strength, visualized by the Q-criterion colored by the instantaneous velocity in the x-direction. Jeong and Hussain [36] originally introduced the Q-criterion to visualize a vortex, and it is defined as $Q = \frac{1}{2}(||\Omega||^2 - ||S||^2)$ where Ω and S are rotation and strain rate tensors, respectively. It can be inferred that the resolution satisfies the requirement for minimum streaks (at least four streaks) to ensure that the flow is not confined in the spanwise direction (Jimenez et al. [37]). It is evident that there are many small-scale vortices, especially in the near-wall region. Large-scale structures develop away from the wall. As expected, those vortical structures, known as hairpins, with various sizes and strengths exist mainly in the logarithmic region.

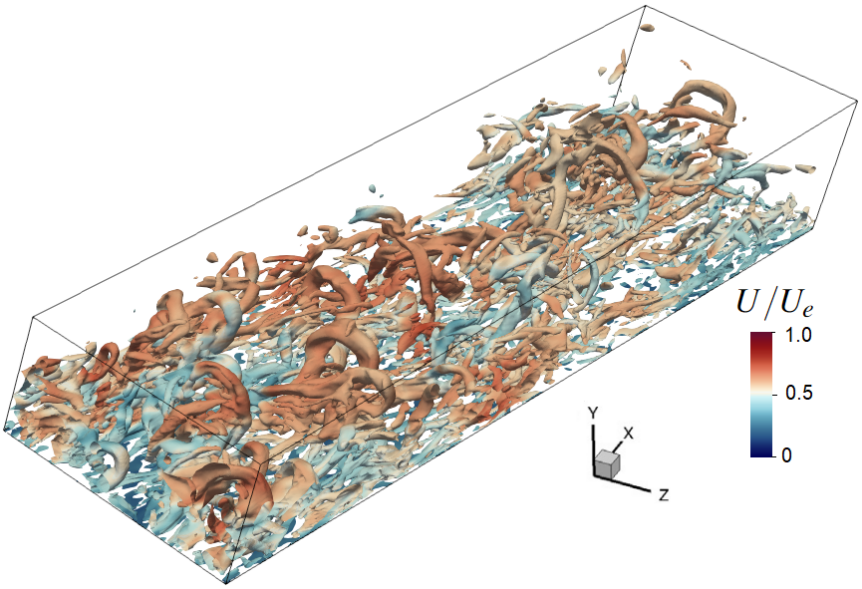

Figure 2. Iso-surface of normalized Q-criterion, $\frac{Q}{\frac{1}{2}|\overline{\Omega}^2_{max}|} = 0.2$, colored by velocity in x-direction.

2. Results

The minimization procedure leads to the turbulent boundary layer parameter values in Table 2. The u_e/u_τ values in Table 2 column 3 is calculated using the velocity scaling law with the optimal parameters for each case. The values are in excellent agreement with DNS predicted values. A nearly continuous increase in the inner layer parameters, (m, κ), can be seen for both moderate blowing cases, $B = 1, 2, 3, 6$, and high blowing cases, $B = 10, 14, 20$. Slight

variation can be seen in outer flow parameters, (b, α) in moderate blowing rates, and generally, outer parameters are higher for those high blowing rates. Qualitatively, the parameters (b, α) depend weakly on the blowing rate at high wall-blowing cases.

Table 2. Blowing rates, optimal model parameters for surface blowing turbulent boundary layer datasets.

B	$(u_e/u_\tau)_{dns}$	$(u_e/u_\tau)_{model}$	m	κ	c	b	α
1	27.559	27.544	1.189	0.390	34.0	5.625	0.381
2	28.290	28.279	1.235	0.396	33.5	4.731	0.405
3	29.921	29.873	1.240	0.404	33.0	3.750	0.461
6	30.985	30.732	1.392	0.415	32.5	5.391	0.583
mean			1.264	0.411	33.5	4.874	0.458
10	31.676	31.846	1.784	0.430	30.0	6.661	0.701
14	32.666	32.908	2.163	0.443	27.0	7.041	0.732
20	34.432	35.034	2.550	0.452	24.0	6.463	0.810
mean			2.166	0.442	27.0	6.722	0.748

The simulation data, with a comparison to the universal velocity profile in Eq. (25), using optimal parameters (dashed line) and mean values of the parameters (solid line) for various blowing rates accompanied by 95% confidence intervals are shown in Fig. 3. Confidence intervals of profiles generated from mean values communicate variation around the profiles. It can be seen that increasing wall-normal blowing strongly modifies the shape of the boundary layer's mean velocity profile. The graphs have distinct logarithmic portions. The effect of increasing the blowing rate on the flow is apparent; the level of the logarithmic region decreases with increasing injection rates. The data from optimal parameters exhibit well-defined wake regions among all blowing rates. The largest errors in the profile, estimated to be on the order of 0.5 in units of U^+, tend to occur in the inner region for $10 < y^+ < 100$. In addition, the error in the logarithmic region for the highest blowing case, $B = 20$, is more pronounced. The error could be due to a slight overestimation of the velocity gradient as the flow transitions from the buffer layer to the logarithmic layer for high blowing cases. Nevertheless, the fit for this region is acceptable; the velocity scaling law profile accurately fits the entire dataset very well. The outer scaling well defines the wake region of the boundary layer for all blowing cases. Furthermore, the profiles generated by mean parameter values, predict the inner layer close to the predictions from optimal parameters with comparatively narrow confidence intervals. This indicates that the inner parameters (b, α) depend weakly on the blowing rate, whereas the sensitivity to the outer parameters is more pronounced. By using the mean parameter values, the range of confidence intervals becomes wider in the wake region contrary to the inner region

confidence level, even for low blowing rates. Namely, the level of confidence in using mean values decreases in the outer layer, especially for the highest blowing rate, $B = 20$.

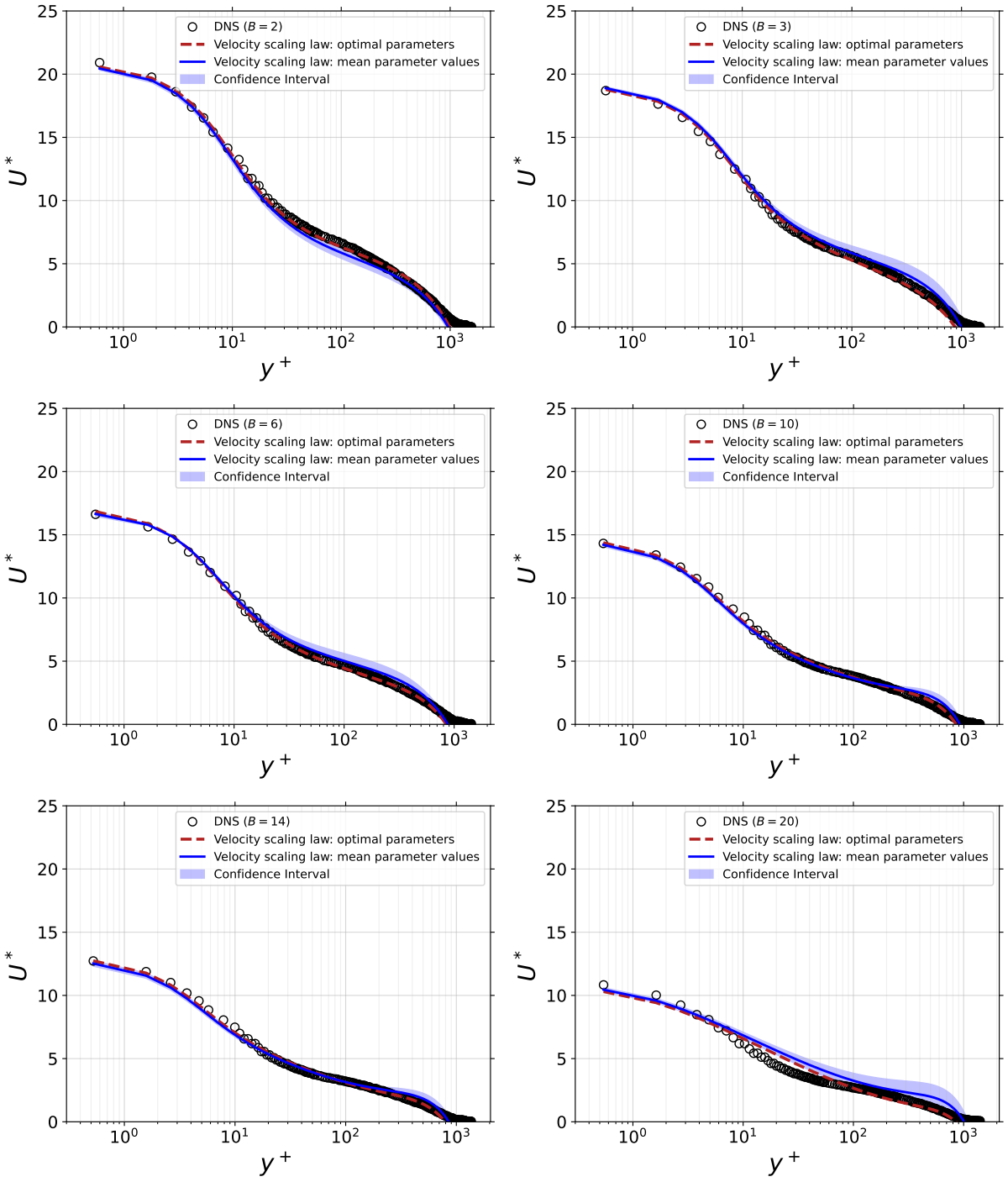

Figure 3. Velocity scaling law of various blowing rates compared to DNS. The dashed lines show the profiles using optimal parameters. The solid line show profiles using mean parameter values.

III. Turbulence Energy Equation Model for Blowing Surfaces

A. Mean Turbulent Kinetic Energy Budget

In the fully developed compressible turbulent flowfield, the budget equation for the turbulent kinetic energy k leads to,

$$0 = -\rho V\frac{\partial k}{\partial y} - \overline{\rho u'v'}\frac{\partial U}{\partial y} - \mu\overline{\frac{\partial u'}{\partial y}\frac{\partial u'}{\partial y}} + \frac{\partial}{\partial y}\left[\mu\frac{\partial k}{\partial y} + \frac{1}{2}\overline{\rho u'u'v'} - \overline{p'v'}\right]. \tag{28}$$

where $-\overline{\rho u'v'}\frac{1\partial U}{\partial y}$ and $\mu\overline{\frac{\partial u'}{\partial y}\frac{\partial u'}{\partial y}}$ are production and dissipation rates of the mean turbulent kinetic energy respectively [38]. Fig. 4(a) shows the $k^+ = k/u_\tau^2$ for various DNS data of blowing parameters. Note, the zero-blowing ($B = 0$) case is also plotted for reference. The peak of k for a turbulent boundary layer with no mass transfer is estimated to occur at $y^+ \approx 11$ [39]; however, for surfaces with mass transfer, the peak continues to shift away from the wall as the blowing rate is increased and for $B = 20$ the maximum location approaches $y^+ \approx 32$. A relatively sharp jump can be seen in the magnitude of k^+ from $B = 3$ to $B = 6$. From $B = 10$ to $B = 20$, the peak of turbulent kinetic energy increases by 8%, however, it shifts drastically from $y^+ \approx 18$ to $y^+ \approx 32$. In the vicinity of the wall, $y^+ < 6$, lower blowing rates experience higher turbulent kinetic energy values, whereas the magnitude of turbulent kinetic energy increases by blowing rates in both the inner and outer layers. For high blowing cases, the change in k^+ with the blowing rate is less significant. The Reynolds shear stress distribution over the boundary layer, $\tau^+ = -\overline{\rho u'v'}/u_\tau^2$, shows a similar trend in Fig. 4(b). Near the wall, damping drives shear stress from zero to high order in y^+ in the viscous wall layer. The maximum position of τ^+ occurs approximately at the beginning of the log layer for no blowing surfaces [40, 41]. Near the log layer, the viscous term in the momentum equation becomes negligible. However, with the surface mass transfer added, the maximum location occurs at a higher y^+, and the effective region of Reynolds shear stress expands remarkably in the boundary layer. These results show the extension of the sublayer with surface blowing rates.

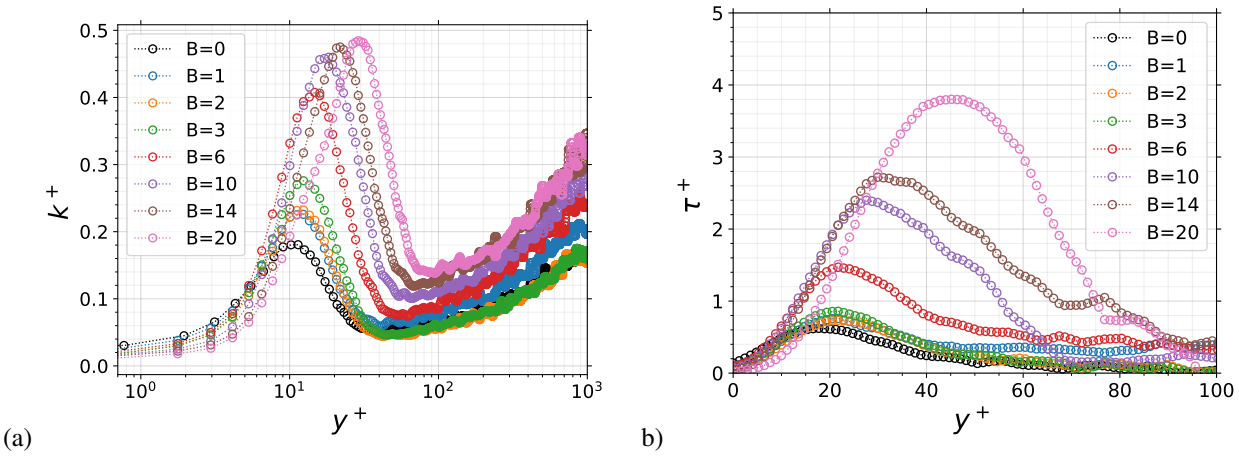

Figure 4. (a) Turbulent kinetic energy budget, k^+, for various blowing, (b) distribution of Reynolds shear stress, τ^+, for various blowing.

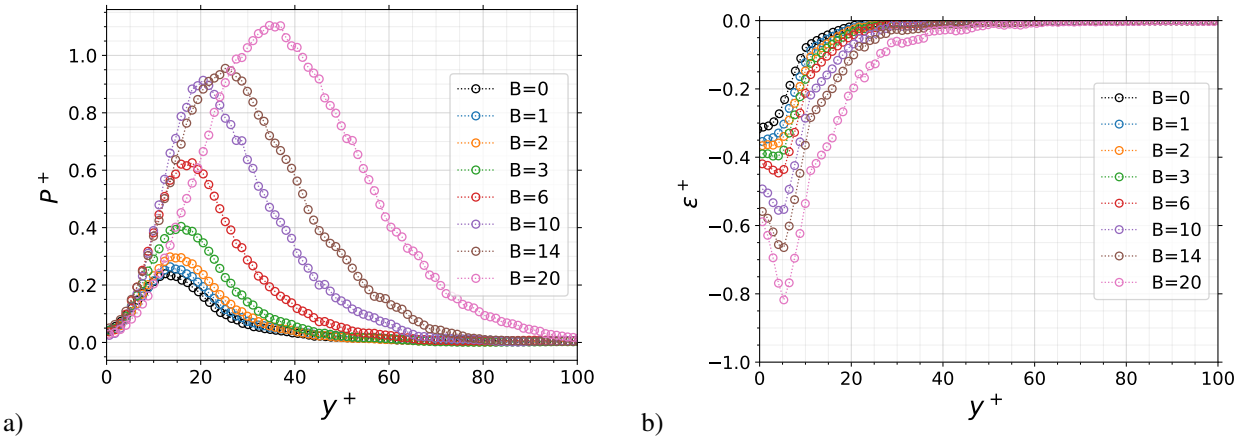

Figure 5. (a) Budget of turbulent kinetic energy production rate, P^+, for various blowing, (b) budget of turbulent kinetic energy dissipation rate, ϵ^+, for various blowing.

With the mass injection, the maximum value of the production term, $P^+ = P/u_\tau^4$, increases by the blowing rate as depicted in Fig. 5(a). For no blowing turbulent boundary layers, the maximum turbulent kinetic energy production rate occurs where $dU^+/dy^+ = 1/2$ and the value of the peak is $P^+ = 1/4$[42, 43]; however, it can be seen that for the case of high blowing, $B = 20$, this value is increased by four times. This must be due to increased Reynolds shear stress, $-\overline{\rho u' v'}$. Although the highest rate of turbulent kinetic energy production occurs very close to the wall, as shown in Fig. 5(a), a substantial fraction of the total turbulent kinetic energy generated is produced in the outer layer $y^+ > 100$. For all blowing rates, more than 25% of the total turbulent kinetic energy is generated in the wake region as shown in Fig. 5(a). The production region extends significantly in the sublayer by the blowing rate. Fig. 5(b) depicts the dissipation rate, ϵ^+. The magnitude of the dissipation rate correlates with surface mass injection rates. A maximum begins to develop in the vicinity of the wall with increasing mass injection at moderate blowing rates. The extremas become more pronounced at

high blowing rates; however, the location of the maxima is consistent among all blowing rates. Sufficiently away from the wall ($y^+ > 30$), the production term balances qualitatively with the dissipation term for moderate blowing rates as can be expected in turbulent boundary layer [44, 45]. At high blowing cases, this balance develops at higher y^+, which could be due to the extension of the sublayer.

In Fig. 6(a), the velocity gradient is plotted in log–log coordinates showing the position of the wake region as B increases. By approaching the free stream, $y^+ > 10$, the velocity gradient drops rapidly in buffer and log layer regions. In the outer layer, approximately $y^+ > 200$, a rapid jump in the velocity gradient occurs at higher blowing rates. In Fig. 6(b), by comparing the log indicator functions of the velocity scaling profile at various blowing rates of the data, only a single maximum appears. This indicates the lower sensitivity to small variations in the wall parameters (κ, m) in the viscous wall layer below $y^+ \approx 20$. A distinguishable difference in log indicator functions appears in the wake region, $y^+ > 500$. The curves depart from one another at the inner boundary of the wake layer. This means the sensitivity to the outer parameters is more pronounced as also indicated in Fig. 3.

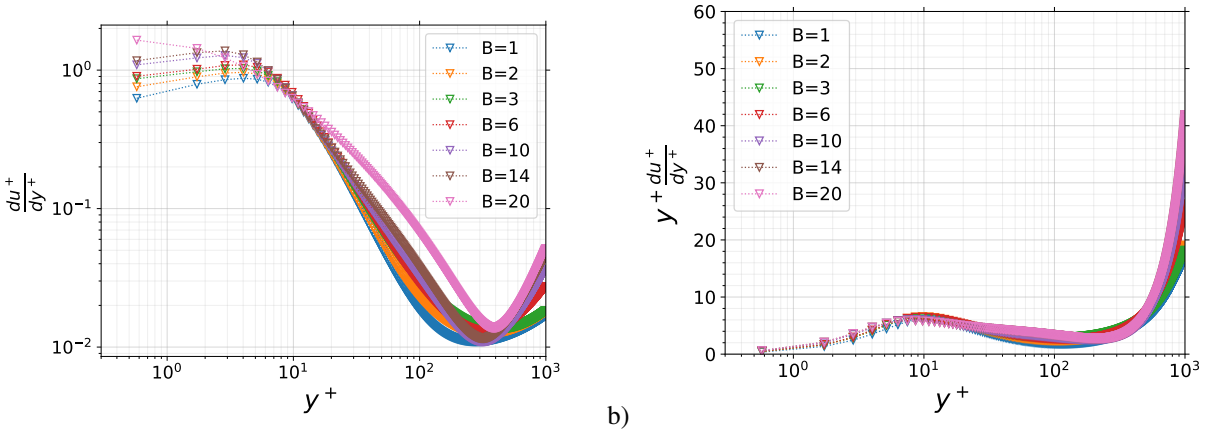

Figure 6. (a) Velocity gradient and (b) log indicator function at various blowing rates.

B. Eddy Viscosity Model for Blowing Surfaces

The eddy viscosity hypothesis is a core element of a mathematical model that describes turbulent flow next to a solid wall [46, 47]. To complete the closure of the turbulence kinetic energy equation, Prandtl introduced a closure coefficient, C_D, for the dissipation rate [48],

$$\epsilon = \frac{C_D k^{3/2}}{l}. \tag{29}$$

According to the turbulence viscosity hypothesis in the boundary layer [49], the approximation for the production rate is,

$$P = \frac{\mu_t}{\rho}(\frac{\partial U}{\partial y})^2. \tag{30}$$

Thus the energy equation model appears as [50],

$$0 = P - \epsilon + \frac{\partial}{\partial y}\left[(\frac{\mu}{\rho} + \frac{\mu_t}{\rho})\frac{\partial k}{\partial y}\right], \tag{31}$$

where the eddy viscosity is,

$$\mu_t = \rho k^{1/2} l, \tag{32}$$

where l is the turbulence length scale, assuming the Prandtl mixing length, $l = \kappa y\,[1 - exp(-y^+/A^+)]$. The eddy viscosity is plotted using the turbulent kinetic energy from DNS data of various blowing parameters in Fig. 7. It can be seen that there is a crest in the inner layer of the boundary layer due to the extrema in the turbulent kinetic energy for blowing surfaces. The crest becomes distinctive for $B = 6$ as shown in Fig. 7(a). It becomes more pronounced for the high blowing cases in Fig. 7(b). The curve of μ_t^+ slightly shifts up by the blowing rate. It is well established that the eddy distribution has strong effects on the momentum and heat transfer rate near the wall in turbulent boundary layers, particularly in buffer regions where both viscous and inertial effects become important. Therefore any velocity distribution in the buffer zone is reduced to finding an adequate eddy viscosity model. [37, 51] An effective eddy viscosity model is required for surfaces with mass transfer since models developed for non-blowing boundary layers may not compare with blowing surfaces. To address this problem, we develop an eddy viscosity formulation based on the near-wall turbulent kinetic energy with the aid of DNS data.

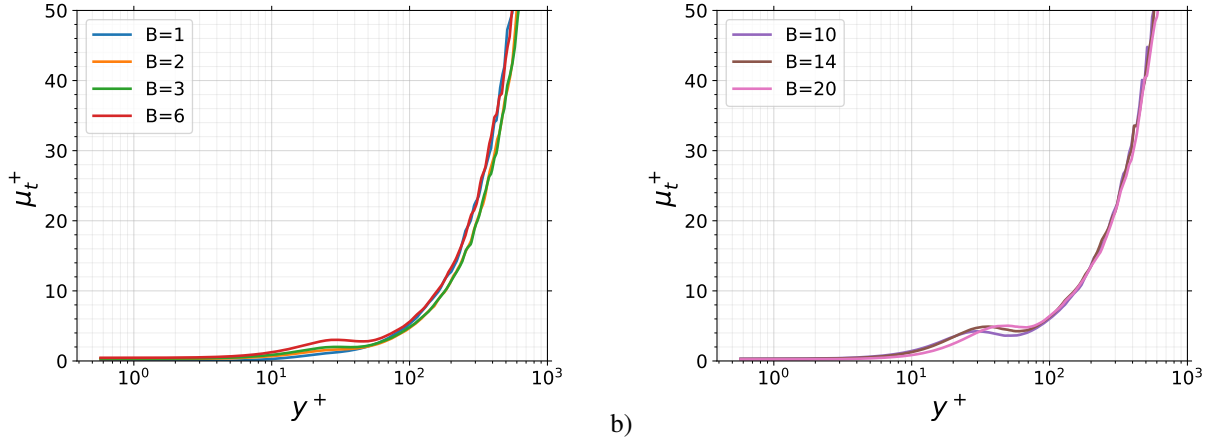

Figure 7. Eddy viscosity calculated from DNS data for a) moderate b) high blowing rates.

We separately derive a turbulent kinetic energy equation for the near-wall and log layer regions. For the near-wall region, the measurements of Sukhodolov et al. [52] approximated the production and dissipation rates from experimental data as:

$$P = C_p \frac{u_\tau^3 \delta}{y^2}, \tag{33}$$

$$\epsilon = C_\epsilon \frac{u_\tau^3 \delta}{y^2}, \tag{34}$$

where C_ϵ and C_p are constants. From Eqs. (33) and (34), $P - \epsilon$ in Eq. (31) can be approximated as:

$$P - \epsilon = C \frac{u_\tau^3 \delta}{y^2}. \tag{35}$$

In addition, Nezu and Nakagawa [53] derived an approximation for the eddy viscosity, μ_t as:

$$\mu_t = C_t \frac{\rho u_\tau^3 \delta}{k}. \tag{36}$$

Substituting in Eq. (31) leads to,

$$-\frac{\partial}{\partial y}\left[(\frac{\mu}{\rho} + C_t \frac{u_\tau^3 \delta}{k})\frac{\partial k}{\partial y}\right] = C \frac{u_\tau^3 \delta}{y^2}. \tag{37}$$

Integrating Eq. (37) and rewriting in wall variables gives,

$$k^+ = D(y^+)^2 e^{-y^+/A_k^+}, \tag{38}$$

where D and $A_k^+ = \rho \delta u_\tau / 2\mu$ are coefficients. For the log layer region, however, one can assume dissipation and production of turbulent kinetic energy are balanced, $P = \epsilon$ [50]. Therefore, the mean momentum and k equations in the log layer region simplify to,

$$0 = \frac{\partial}{\partial y}\left[\frac{\mu_t}{\rho}\frac{\partial U}{\partial y}\right], \tag{39}$$

$$0 = \frac{\mu_t}{\rho}(\frac{\partial U}{\partial y})^2 - \frac{C_D k^{3/2}}{l}. \tag{40}$$

We seek the condition under which these simplified equations yield a solution consistent with the law of the wall. The solution yields an equation for turbulent kinetic energy in the outer layer,

$$k^+ = \frac{1}{C_D}\left[\frac{V_w^+}{4\kappa} ln y^+ + C'\right]^2, \tag{41}$$

where C' is a coefficient and can be verified from the upper limit of the buffer layer in Eq. (38) for each blowing case.

Table 3. Values of coefficient D obtained from Eq. (38) and DNS data.

B	1	2	3	6	10	14	20
D	0.0613	0.0579	0.0550	0.0513	0.0481	0.0466	0.0443

The coefficient in the turbulent kinetic energy formulation for the inner layer, Eq. (38), must be verified using DNS data of various blowing parameters since it depends on both C_ϵ and C_p. Examination of Eq. (38) by DNS data shows that D is blowing rate dependent. Table 3 gives values of $D(B)$ obtained from Eq. (38) and DNS data of various blowing rates. The values drop slightly by increasing the surface mass transfer. A logarithmic fit is suggested for the coefficient when turbulent kinetic energy varies by Reynolds number [54], $D = R_1 \ln B + R_2$. Fig. 8 shows a logarithmic function that perfectly fits the coefficient D values for blowing cases also, with $R_1 = 0.0057$ and $R_2 = 0.0614$.

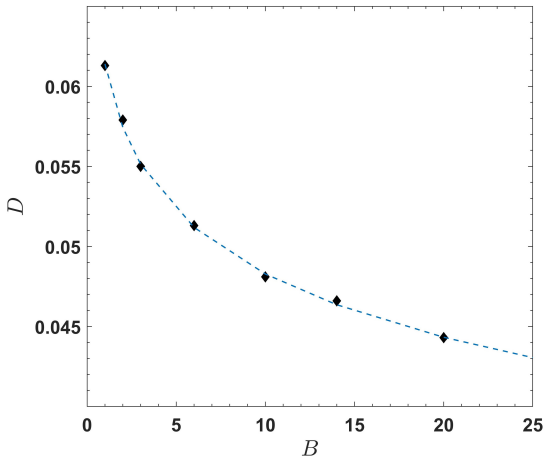

Figure 8. Dependency of the coefficient D on the blowing rate, values obtained from DNS data; proposed fit is $D(B) = 0.0057 \ln B + 0.0614$ **and** R^2**= 0.9983.**

Figures 9(a) and (b) depict the modeled turbulent kinetic energy from Eq. (38) and (41), which combine the inner and outer regions for moderate to high blowing cases. The logarithmic behavior of turbulent kinetic energy in the outer layer, shown in Eq. (41), is apparent from Fig. 9(a). The slope increases slightly with the mass transfer value, V_w^+, as Eq. (41) indicates. Similar to DNS results, the maximum of the modeled turbulent kinetic energy occurs at the beginning of the buffer region and moves away from the wall with increasing the blowing rate. The magnitude of k^+ increases with surface mass transfer, and there is a jump from $B = 3$ to $B = 6$, consistent with results revealed by DNS

in Fig. 4(a). The sublayer extends quite remarkably with mass transfer values at moderate blowing rates. Namely, the logarithmic region of k^+, predicted by Eq. (41) starts at $y^+ \approx 40$ and $y^+ \approx 100$ for $B = 1$ and $B = 6$, respectively. For high blowing cases, shown in Fig. 9(b), increasing k^+ with the blowing rate is less significant. The logarithmic behavior in the outer region is apparent, as predicted by Eq. (41). Overall, the total turbulent kinetic energy is well predicted in the inner and outer regions. The peak location and maxima errors are less than 5% for all blowing cases.

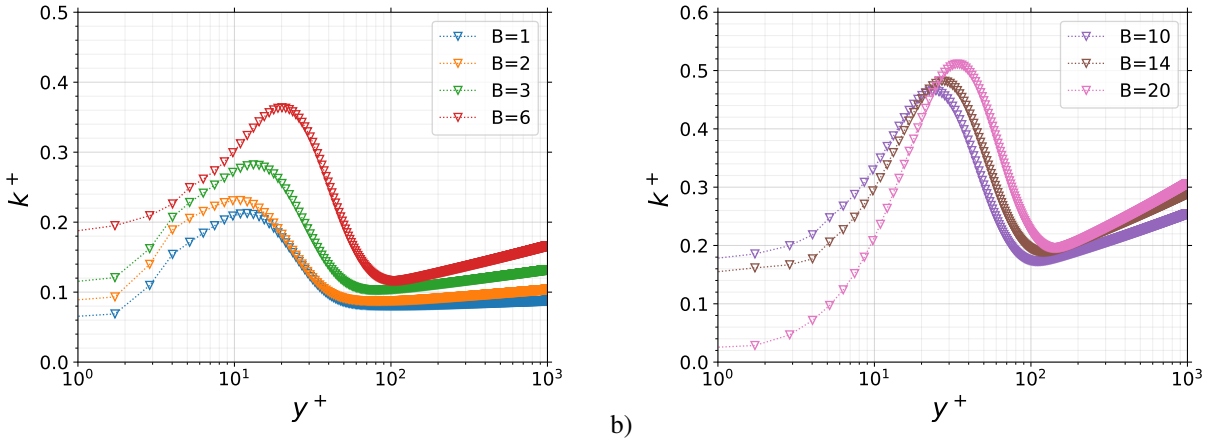

Figure 9. Budget of turbulent kinetic energy predicted by the energy equation model for (a) moderate (b) high blowing rates.

Next, we compute the eddy viscosity from Eq. (32) using modeled turbulent kinetic energy and Prandtl mixing length,

$$\mu_t^+ = \kappa \rho D^{0.5} (y^+)^2 e^{-y^+/2A_k^+} \left[1 - exp(-y^+/A^+)\right]. \tag{42}$$

Figures 10(a) and (b) plot the modeled eddy viscosity for moderate and high blowing cases. A crest starts to develop as the bowing rate increases in Fig. 10(a), and it becomes distinguishable at $B = 6$; higher μ_t^+ is predicted for higher surface mass transfers. These results are consistent with μ_t^+ computed from DNS data in Fig. 7. For high blowing cases shown in Fig. 10(b), the crest is more pronounced in the buffer region; however, the profile is less sensitive to the surface mass transfer increment. The trend is similar to DNS predicted eddy viscosity for high blowing cases. As the results show, the eddy distribution differs from non-blowing surfaces in the buffer region, where viscous and inertial effects become important. Therefore a functional model for surfaces with mass transfer could predict the velocity distribution more accurately.

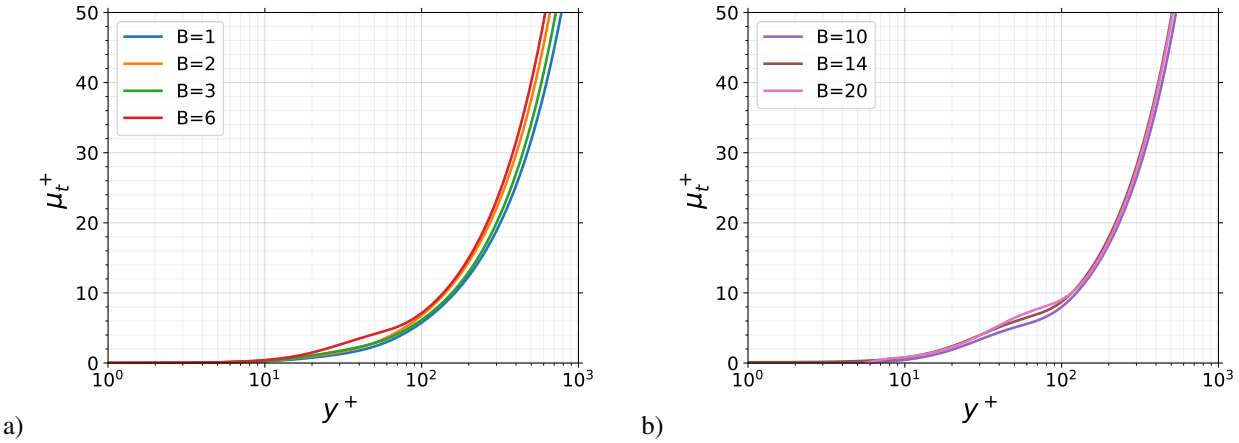

Figure 10. Eddy viscosity predicted by Eq. (42) for (a) moderate (b) high blowing rates.

IV. Conclusion

A new scaling law is developed for turbulent boundary layers with high surface mass transfers. An analytical model is developed and scaled with DNS data of various blowing rates. Emphasis is placed on moderate to high mass transfer rates, which are relevant to the most common hybrid rocket configurations. Results from DNS show wall-normal blowing strongly modifies the shape of the boundary layer mean velocity profile. DNS data is used to establish a functional law of the wall and a law of wake by means of the relation between the wall shear stress and surface mass transfer. For the first time, the mean turbulent kinetic energy budget was analyzed for various blowing rates. Results show wall-blowing enhances the intensity of the velocity fluctuations; the Reynolds shear stress extends remarkably in the inner boundary region. For the higher blowing case, the production rate of turbulent kinetic energy increases by four times, and the location of the extrema shifts away from the wall due to the extension of the sublayer.

The eddy viscosity calculated from DNS data shows a crest develops in the buffer region as the surface mass transfer increases and becomes more pronounced for high wall-blowing cases. Therefore, an eddy viscosity model is derived and scaled using DNS data. The predicted turbulent kinetic energy and eddy viscosity agree with DNS data for moderate to high surface mass transfer. The proposed model can be used to develop appropriate wall models for wall-modeled LES of turbulent boundary layers involving surface mass injections.

Acknowledgments

This research is funded by the United States Department of Energy's (DoE) National Nuclear Security Administration (NNSA) under the Predictive Science Academic Alliance Program III (PSAAP III) at the University at Buffalo, under contract number DE-NA0003961.

The authors wish to thank the reviewers for their constructive comments and suggestions for improving the manuscript.

Conflict of interest

The authors have no conflicts to disclose.

AVAILABILITY OF DATA

The data that support the findings of this study are available from the corresponding author upon reasonable request.

References

[1] Budzinski, K., Aphale, S. S., Ismael, E. K., Surina, G., and DesJardin, P. E., "Radiation heat transfer in ablating boundary layer combustion theory used for hybrid rocket motor analysis," *Combustion and Flame*, Vol. 217, 2020, pp. 248–261.

[2] Karabeyoglu, M. A., Altman, D., and Cantwell, B. J., "Combustion of Liquefying Hybrid Propellants: Part 1, General Theory," *Journal of Propulsion and Power*, Vol. 18, No. 3, 2002, pp. 610–620. https://doi.org/10.2514/2.5975.

[3] Karabeyoglu, A., Zilliac, G., Cantwell, B., Zilwa, S., and Castelluci, P., "Scale-up Tests of High Regression Rate Liquefying Hybrid Rocket Fuels," *Spacecraft and Rockets*, 2003. https://doi.org/10.2514/6.2003-1162.

[4] Van Driest, E. R., "On Turbulent Flow Near a Wall," *Journal of the Aeronautical Sciences*, Vol. 23, No. 11, 1956, pp. 1007–1011. https://doi.org/10.2514/8.3713.

[5] Kays, W. M., Moffat, R. J., and Thielbahr, W. H., "Heat Transfer to the Highly Accelerated Turbulent Boundary Layer With and Without Mass Addition," *Journal of Heat Transfer*, Vol. 92, No. 3, 1970, pp. 499–505.

[6] Nicoll, W. B., Strong, A. B., and Woolner, K. A., "On the Laminar Motion of a Fluid Near an Oscillating Porous, Infinite Plane," *Journal of Applied Mechanics*, Vol. 35, No. 1, 1968, pp. 164–166. https://doi.org/10.1115/1.3601134, URL https://doi.org/10.1115/1.3601134.

[7] Tennekes, H., "Similarity laws for turbulent boundary layers with suction or injection," *Journal of Fluid Mechanics*, Vol. 21, No. 4, 1965, p. 689–703. https://doi.org/10.1017/S0022112065000423.

[8] Cebeci, T., and Smith, A. M. O., "A Finite-Difference Method for Calculating Compressible Laminar and Turbulent Boundary Layers," *Journal of Basic Engineering*, Vol. 92, No. 3, 1970, pp. 523–535.

[9] Mickley, H. S., and Davis, R. S., "Momentum Transfer for Flow Over a Flat Plate with Blowing." *In Tech. Rep. vol. 4017, MIT.*, 1957.

[10] Black, T. J., and S Arnecki, A. J., "Momentum Transfer for Flow Over a Flat Plate with Blowing." *Rep. 20, Cambridge University, Engineering Department.*, 1958.

[11] Stevenson, T. N., "A modified velocity defect law for turbulent boundary layers with injection." *Tech. Rep. 170 The College of Aeronautics Cranfield.*, 1963.

[12] Marxman, G., and Gilbert, M., "Turbulent boundary layer combustion in the hybrid rocket," *Symposium (International) on Combustion*, Vol. 9, No. 1, 1963, pp. 371–383. https://doi.org/https://doi.org/10.1016/S0082-0784(63)80046-6.

[13] Marxman, G. A., "Combustion in the turbulent boundary layer on a vaporizing surface," *Symposium (International) on Combustion*, Vol. 10, No. 1, 1965, pp. 1337–1349. https://doi.org/https://doi.org/10.1016/S0082-0784(65)80268-5, tenth Symposium (International) on Combustion.

[14] Andersen, P. S., Kays, W. M., and Moffat, R. J., "The turbulent boundary layer on a porous plate: An experimental study of the fluid mechanics for adverse free stream pressure gradients." *Tech. Rep. CR 127817. NASA.*, 1972.

[15] Squire, L. C., "A law of the wall for compressible turbulent boundary layers with air injection," *Journal of Fluid Mechanics*, Vol. 37, No. 3, 1969, p. 449–456. https://doi.org/10.1017/S0022112069000656.

[16] Ferro, M., "Experimental study on turbulent boundary-layer flows with wall transpiration." *PhD dissertation, KTH Mechanics, Royal Institute of Technology*, 2017.

[17] Sumitani, Y., and Kasagi, N., "Direct numerical simulation of turbulent transport with uniform wall injection and suction," *AIAA Journal*, Vol. 33, No. 7, 1995, pp. 1220–1228. https://doi.org/10.2514/3.12363.

[18] Vigdorovich, I., and Oberlack, M., "Analytical study of turbulent Poiseuille flow with wall transpiration," *Physics of Fluids*, Vol. 20, No. 5, 2008.

[19] Avsarkisov, V., Oberlack, M., and Hoyas, S., "New scaling laws for turbulent Poiseuille flow with wall transpiration," *Journal of Fluid Mechanics*, Vol. 746, 2014, p. 99–122. https://doi.org/10.1017/jfm.2014.98.

[20] Avsarkisov, V. S., Oberlack, M., and Khujadze, G., "Turbulent Poiseuille Flow with Wall Transpiration: Analytical Study and Direct Numerical Simulation," *Journal of Physics: Conference Series*, Vol. 318, No. 2, 2011, p. 022004. https://doi.org/10.1088/1742-6596/318/2/022004.

[21] Piomelli, U., Ferziger, J., Moin, P., and Kim, J., "New approximate boundary conditions for large eddy simulations of wall-bounded flows," *Physics of Fluids A: Fluid Dynamics*, Vol. 1, No. 6, 1989, pp. 1061–1068. https://doi.org/10.1063/1.857397.

[22] Bose, S. T., and Park, G. I., "Wall-Modeled Large-Eddy Simulation for Complex Turbulent Flows," *Annual Review of Fluid Mechanics*, Vol. 50, No. 1, 2018, pp. 535–561. https://doi.org/10.1146/annurev-fluid-122316-045241.

[23] Larsson, J., Kawai, S., Bodart, J., and Bermejo-moreno, I., "Large eddy simulation with modeled wall-stress: recent progress and future directions," *Mechanical Engineering Reviews*, Vol. 3, No. 1, 2016, pp. 15–00418–15–00418. https://doi.org/10.1299/mer.15-00418.

[24] Lv, Y., Huang, X. L. D., Yang, X., and Yang, X. I. A., "Wall-model integrated computational framework for large-eddy simulations of wall-bounded flows," *Physics of Fluids*, Vol. 33, No. 12, 2021, p. 125120. https://doi.org/10.1063/5.0073506.

[25] Park, G. I., and Moin, P., "Space-time characteristics of wall-pressure and wall shear-stress fluctuations in wall-modeled large eddy simulation," *Phys. Rev. Fluids*, Vol. 1, 2016, p. 024404. https://doi.org/10.1103/PhysRevFluids.1.024404.

[26] Pour Razaghi, M. J., Rezaei Sani, S. M., Masoumi, Y., Huang, G., and Li, H., "Comparison and modification of turbulence models for active flow separation control over a flat surface," *Physics of Fluids*, Vol. 35, No. 6, 2023, p. 065125. https://doi.org/10.1063/5.0151815.

[27] Venugopal, P., Moser, R. D., and Najjar, F. M., "Direct numerical simulation of turbulence in injection-driven plane channel flows," *Physics of Fluids*, Vol. 20, No. 10, 2008.

[28] Coles, D., "The law of the wake in the turbulent boundary layer," *Journal of Fluid Mechanics*, Vol. 1, No. 2, 1956, p. 191–226. https://doi.org/10.1017/S0022112056000135.

[29] Cantwell, B. J., "Integral measures of the zero pressure gradient boundary layer over the Reynolds number range," *Physics of Fluids*, Vol. 33, No. 8, 2021, p. 085108. https://doi.org/10.1063/5.0061535.

[30] Subrahmanyam, M. A., Cantwell, B. J., and Alonso, J. J., "A universal velocity profile for turbulent wall flows including adverse pressure gradient boundary layers," *Journal of Fluid Mechanics*, Vol. 933, 2022, p. A16. https://doi.org/10.1017/jfm.2021.998.

[31] Klein, M., and Sadiki, A., "A digital filter based generation of inflow data for spatially developing direct numerical or large eddy simulations," *Journal of Computational Physics*, Vol. 166, No. 2, 2003, pp. 652–665.

[32] "ABLATE Ablative Boundary Layers At The Exascale," https://ubchrest.github.io/ablate/, 2021.

[33] Liou, M.-S., "A sequel to AUSM, Part II: AUSM+-up for all speeds," *Journal of Computational Physics*, Vol. 214, No. 1, 2006, pp. 137–170. https://doi.org/https://doi.org/10.1016/j.jcp.2005.09.020.

[34] Sementilli, M., McGurn, M., and Chen, J., "A Scalable Compressible Volume of Fluid Solver using a Stratified Flow Model," *International Journal for Numerical Methods in Fluids*, 2022. https://doi.org/10.1002/fld.5169.

[35] Sementilli, M. L., McGurn, M., and Chen, J. M., "A Scalable Multiphase Flow Solver for Simulation of Hybrid Rocket Motors," *AIAA SCITECH 2023 Forum*, 2023. https://doi.org/10.2514/6.2023-0279.

[36] Jeong, J., and Hussain, F., "On the identification of a vortex," *Journal of Fluid Mechanics*, Vol. 285, No. 3, 2000, pp. 69–94.

[37] Jiménez, J., and Moin, P., "The minimal flow unit in near-wall turbulence," *Journal of Fluid Mechanics*, Vol. 225, 1991, p. 213–240. https://doi.org/10.1017/S0022112091002033.

[38] Pope, S. B., *Turbulent Flows*, Cambridge University Press, 2000. https://doi.org/10.1017/CBO9780511840531.

[39] Inoue, M., and Pullin, D. I., "Large-eddy simulation of the zero-pressure-gradient turbulent boundary layer up to Re= O(1012)," *Journal of Fluid Mechanics*, Vol. 686, 2011, p. 507–533. https://doi.org/10.1017/jfm.2011.342.

[40] Chen, X., and Sreenivasan, K. R., "Reynolds number scaling of the peak turbulence intensity in wall flows," *Journal of Fluid Mechanics*, Vol. 908, 2021, p. R3. https://doi.org/10.1017/jfm.2020.991.

[41] Clauser, F. H., *The Turbulent Boundary Layer*, Advances in Applied Mechanics, Vol. 4, Elsevier, 1956. https://doi.org/https://doi.org/10.1016/S0065-2156(08)70370-3.

[42] She, Z.-S., Chen, X., and Hussain, F., "Quantifying wall turbulence via a symmetry approach: a Lie group theory," *Journal of Fluid Mechanics*, Vol. 827, 2017, p. 322–356. https://doi.org/10.1017/jfm.2017.464.

[43] Cantwell, B. J., "A universal velocity profile for smooth wall pipe flow," *Journal of Fluid Mechanics*, Vol. 878, 2019, pp. 834 – 874.

[44] Perry, A. E., and Marušić, I., "A wall-wake model for the turbulence structure of boundary layers. Part 1. Extension of the attached eddy hypothesis," *Journal of Fluid Mechanics*, Vol. 298, 1995, p. 361–388. https://doi.org/10.1017/S0022112095003351.

[45] Scarano, F., Jacob, M. C., Carbonneau, X., and Gowree, E. R., "On the turbulent boundary layer over a flat plate at moderate Reynolds numbers," *Physics of Fluids*, Vol. 34, No. 11, 2022, p. 115150. https://doi.org/10.1063/5.0124498.

[46] Cheikh, M. I., Chen, J., and Wei, M., "Small-scale energy cascade in homogeneous isotropic turbulence," *Phys. Rev. Fluids*, Vol. 4, 2019, p. 104610. https://doi.org/10.1103/PhysRevFluids.4.104610.

[47] Katopodes, N. D., "Chapter 8 - Turbulent Flow," *Free-Surface Flow*, edited by N. D. Katopodes, Butterworth-Heinemann, 2019, pp. 566–650. https://doi.org/https://doi.org/10.1016/B978-0-12-815489-2.00008-3.

[48] Cazalbou, J. B., and Bradshaw, P., "Turbulent transport in wall-bounded flows. Evaluation of model coefficients using direct numerical simulation," *Physics of Fluids A: Fluid Dynamics*, Vol. 5, No. 12, 1993, pp. 3233–3239.

[49] Blazek, J., "Chapter 7 - Turbulence Modelling," *Computational Fluid Dynamics: Principles and Applications (Second Edition)*, edited by J. Blazek, Elsevier Science, Oxford, 2005, second edition ed., pp. 227–270. https://doi.org/https://doi.org/10.1016/B978-008044506-9/50009-6.

[50] Wilcox, D., *Turbulence Modeling for CFD*, No. v. 1 in Turbulence Modeling for CFD, DCW Industries, 2006.

[51] Zangeneh, R., "Data-driven model for improving wall-modeled large-eddy simulation of supersonic turbulent flows with separation," *Physics of Fluids*, Vol. 33, No. 12, 2021, p. 126103. https://doi.org/10.1063/5.0072550.

[52] Sukhodolov, A., Thiele, M., and Bungartz, H., "Turbulence structure in a river reach with sand bed," *Water Resources Research - WATER RESOUR RES*, Vol. 34, 1998, pp. 1317–1334. https://doi.org/10.1029/98WR00269.

[53] Nakagawa, H., and Nezu, I., *Turbulence in Open Channel Flows*, v. 1, Taylor & Francis Group, 1993.

[54] Absi, R., "A simple eddy viscosity formulation for turbulent boundary layers near smooth walls," *Comptes Rendus Mécanique*, Vol. 337, No. 3, 2009, pp. 158–165. https://doi.org/https://doi.org/10.1016/j.crme.2009.03.010.